

# Photoassociation reaction of OH molecules through reverse ladder transition

Yingyu Niu (牛英煜)\* and Rong Wang (王荣)

School of Science, Dalian Jiaotong University, Dalian 116028, China

\*Corresponding author: niuyy@djtu.edu.cn

Received March 1, 2018; accepted April 16, 2018; posted online May 25, 2018

Photoassociation via reverse ladder transition controlled by two and four laser pulses is investigated using the time-dependent quantum wave packet method. The calculated results show that the amplitudes of the pulses have an enormous effect on the target population and total yield of association. For the target state with a high energy level, the population of background states can reduce the state-selectivity. Although, the total yield of association is decreased, the four pulses can induce the population transferring to low vibrational levels, and the state-selectivity of the target state is high.

OCIS codes: 020.4180, 320.5390.

doi: 10.3788/COL201816.060201.

The molecular reaction controlled by laser fields is an interesting and active subject of research<sup>[1-3]</sup>. Significant efforts have been focused on making and breaking molecular chemical bonds, i.e., photoassociation (PA) and photodissociation (PD). In the process of PA, a pair of collision atoms forms a molecule through absorbing or emitting photons when the suitable parameters of pulses are chosen. Many approaches are proposed to achieve the reaction of PA, such as the stimulated Raman adiabatic passage (STIRAP) technique<sup>[4]</sup>, coherent control with shaped laser pulses<sup>[5]</sup>, chirped laser pulses<sup>[6]</sup>, Feshbach-optimized photoassociation<sup>[7]</sup>, and spin-orbit induced photoassociation<sup>[8]</sup>.

According to the distance of two collision atoms, the PA reaction can be divided into long-range PA ( $20a_0 < R < 3000a_0$ ) and short-range PA ( $R < 20a_0$ ), where  $a_0$  is the Bohr radius. For the long-range PA, the collision atoms with low collision energy mainly form alkali-metal molecules, such as Rb<sub>2</sub>, Cs<sub>2</sub>, Li<sub>2</sub>, Na<sub>2</sub>, LiRb, RbCs, NaCs, and LiCs<sup>[9-12]</sup>. The short-range PA for alkali-metal molecules also has been studied both theoretically and experimentally<sup>[13-17]</sup>. The short-range PA with high energy collision has been proposed theoretically and its products include OH, HBr, HF, HI, and NaH<sup>[8,18,19]</sup>. In a PA reaction, the molecules in the ground electronic state can be produced in two-color laser pulses<sup>[20,21]</sup>. There are two steps in this PA process: first, the collision atoms induced by a pump pulse form molecules in the excited electronic state, and then those product molecules are transferred to the ground electronic state induced by a dump pulse. A single pulse can also be employed to produce the molecules in the ground electronic state<sup>[22,23]</sup>. In this process, the pulse induces the collision atoms emitting photons and transferring from continuum states to bound states through permanent dipole moment transition. Korolkov *et al.*<sup>[24]</sup> first proposed the PA reaction of OH molecules and the OH molecules in the state  $|\nu = 15\rangle$  were produced

through the interaction of a permanent dipole moment and an infrared laser pulse. For a thermal gas of atoms, the PA reaction of OH molecules in the ground electronic state, which is induced by a single laser pulse, was investigated in the context of quantum optimal control theory<sup>[25]</sup>. The above studies were based on a one-dimensional model (the rotational freedom degree is neglected). In the two-dimensional (2D) model, the probability of product molecules is obviously reduced<sup>[26]</sup>.

The ladder transition usually takes place in the process of population manipulation<sup>[27-29]</sup>. This transition is composed of the initial, intermediate, and target states, and these three states satisfy the condition  $E_1 < E_2 < E_3$ , where  $E_1$ ,  $E_2$ , and  $E_3$  are the eigenenergies of the initial, intermediate, and target states, respectively. These states are coupled by two or more pulses and the population can be transferred from an initial state in a low energy level to a target state in a high energy level.

In this Letter, we investigate the PA reaction of OH molecules in the 2D model by using the time-dependent quantum wave packet method which is an important tool for investigating the PA<sup>[24,25,30,31]</sup>. The PA reaction is achieved through the reverse ladder transition, as shown in Fig. 1. The two pulses are employed to induce the collision atoms transferring to three different target states via an intermediate state. The four laser pulses are used to obtain the product molecules in the state  $|0, 0\rangle$ , and the reverse ladder transition includes four intermediate states. The relations between the population distributions and the pulse amplitudes are discussed, and the effects of the different target states on the state-selectivity are examined in detail.

In our theoretical model, only the ground electronic state of OH molecule is taken into account. In the Born–Oppenheimer approximation, the 2D time-dependent Schrödinger equation can be expressed as

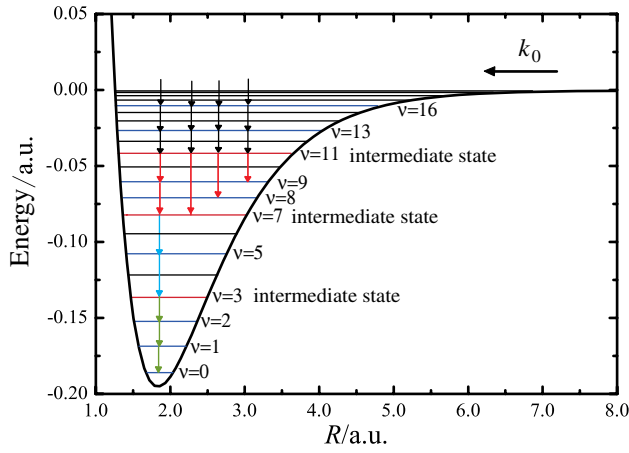


Fig. 1. Processes of the reverse ladder transition.

$$i\hbar \frac{\partial}{\partial t} \Psi(R, \theta, t) = (\hat{H}_{\text{mol}} + \hat{H}_{\text{int}}) \Psi(R, \theta, t), \quad (1)$$

where  $\Psi(R, \theta, t)$  is the nuclear wave function. The molecular Hamiltonian  $\hat{H}_{\text{mol}}$  is written as

$$\hat{H}_{\text{mol}} = -\frac{\hbar^2}{2m} \frac{\partial^2}{\partial R^2} - \frac{\hbar^2}{2mR^2} \frac{1}{\sin \theta} \frac{\partial}{\partial \theta} \left( \sin \theta \frac{\partial}{\partial \theta} \right) + \hat{V}, \quad (2)$$

where  $\theta$  is the angle between the laser electric field axis and the molecular axis, and  $R$  and  $m$  are the internuclear separation and the reduced mass, respectively. The potential energy  $\hat{V}$  of the ground electronic state is described by the Morse potential function<sup>[24]</sup>. The field-molecule interaction  $\hat{H}_{\text{int}}$  is given by

$$\hat{H}_{\text{int}} = -\varepsilon(t) \cos \theta \mu(R), \quad (3)$$

where  $\mu(R)$  is the permanent dipole moment function<sup>[24]</sup>.

The electric field  $\varepsilon(t)$  is obtained by  $\sin^2$ -shaped pulses

$$\varepsilon(t) = \sum_i E_i \sin^2 \left[ \frac{\pi(t - t_i)}{\tau_i} \right] \cos[\omega_i(t - t_i)], \quad (4)$$

where  $E_i$ ,  $\omega_i$ ,  $t_i$ , and  $\tau_i$  are the electric field amplitude, carrier frequency, start time, and duration of the  $i$ th pulse, respectively.

The split operator method<sup>[28,32]</sup> is used to propagate the initial wave packet, which is described by the Gaussian wave packet<sup>[25,26]</sup>. The initial position of the wave packet is optimized for a fixed start time of the first pulse at  $t = 0$ <sup>[24]</sup>, and the optimal position is  $29.0 a_0$ . Here, we assume that the angular momentum quantum number for the initial collision is  $j = 0$ . The time-dependent population  $P_{\nu,j}$  of the rovibrational state can be calculated by projecting the time-dependent wave function  $\Psi(t)$  on the eigenstate  $|\nu, j\rangle$ . Calculating the sum of the populations on the bound states, we can obtain the total yield  $P_{\text{tot}}$  of associated OH molecules.

For a PA reaction induced by a single pulse, the probability of the PA depends on the initial collision energy, the parameters of the pulse, and the rovibrational level of the target state. We have calculated the probability of the PA for different target states in a single pulse. The results show that the product molecules with a high probability can be obtained through 3-photon transition when the state  $|11, 1\rangle$  is chosen as the target state. The corresponding collision energy is  $9.89 \text{ kJ/mol}$  and the pulse parameters are chosen as:  $E_1 = 322.96 \text{ MV/cm}$ ,  $\tau_1 = 0.60 \text{ ps}$ ,  $t_1 = 0 \text{ ps}$ , and  $\omega_1 = 3580.09 \text{ cm}^{-1}$ . The population  $P_{11,1}$  and the total yield  $P_{\text{tot}}$  are  $0.297$  and  $0.351$ , respectively.

We choose the state  $|11, 1\rangle$  as the intermediate state and employ the second pulse to induce the population transferring from the state  $|11, 1\rangle$  to the target state  $|9, 0\rangle$ , as shown in Fig. 1. The reverse ladder transition is as follows:

$$\text{continuum state} \xrightarrow{\omega_1} |16, 1\rangle \xrightarrow{\omega_1} \left\{ \begin{array}{l} |13, 0\rangle \\ |13, 2\rangle \end{array} \right\} \xrightarrow{\omega_1} |11, 1\rangle \xrightarrow{\omega_2} |9, 0\rangle. \quad (5)$$

The parameters of the second pulse are chosen as:  $E_2 = 106.98 \text{ MV/cm}$ ,  $\tau_2 = 0.75 \text{ ps}$ ,  $t_2 = 0 \text{ ps}$ , and  $\omega_2 = 4231.43 \text{ cm}^{-1}$ .

The two overlapping laser pulses and the time-dependent population distributions are shown in Fig. 2. When  $t > 0.15 \text{ ps}$ , there is population in the state  $|16, 1\rangle$ , which is induced by the first pulse, and the population then increases with time. When  $t > 0.35 \text{ ps}$ , the population  $P_{16,1}$  decreases with the increase of  $P_{11,1}$ , which indicates that the population in the state  $|16, 1\rangle$  is transferred to the state  $|11, 1\rangle$  via the states  $|13, 0\rangle$  and  $|13, 2\rangle$ . Because there are large one-photon detunings of the first pulse from the transitions  $|16, 1\rangle \rightarrow |13, 0\rangle$  and  $|16, 1\rangle \rightarrow |13, 2\rangle$ , the populations occurring in the states  $|13, 0\rangle$  and  $|13, 2\rangle$  are very small. When  $t > 0.40 \text{ ps}$ , the second pulse induces the population in the state  $|11, 1\rangle$  transferring to the target state  $|9, 0\rangle$ . As the two pulses are turned off, the populations  $P_{9,0}$  and  $P_{\text{tot}}$  are  $0.224$  and  $0.344$ , and the state-selectivity is  $P_{9,0}/P_{\text{tot}} = 65\%$ . Besides the transition pathway [Eq. (5)], the two pulses can drive the other transitions, and a small amount of population is transferred to the background states, as shown in Fig. 2(c), which reduces the state-selectivity.

The rovibrational population of the product molecules depends on the amplitudes of the pulses. The population variation with the amplitude  $E_1$  is shown in Fig. 3(a). It can be seen that the curves of the populations  $P_{9,0}$  and  $P_{\text{tot}}$  increase first and then decrease with the variation of amplitude. The maximal values of the two curves are both at about  $E_1 = 325 \text{ MV/cm}$ . The time-dependent population distributions for  $E_1 = 200 \text{ MV/cm}$  are shown in Fig. 3(b). Because the amplitude  $E_1$  in Fig. 3(b) is smaller than that in Fig. 2(b), the total yield  $P_{\text{tot}}$  is decreased. Moreover, the smaller amplitude  $E_1$  can reduce the transition

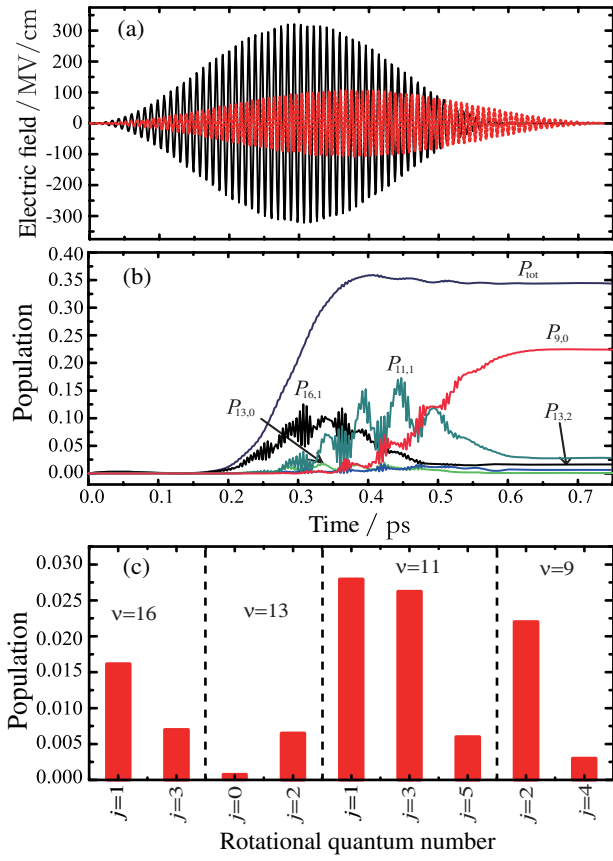


Fig. 2. Process of PA for the target state  $|9,0\rangle$  in two laser pulses. (a) The total electric field of two laser pulses. (b) The time-dependent population distributions for rovibrational states. (c) The population distributions of the intermediate and background states at the end of laser pulses.

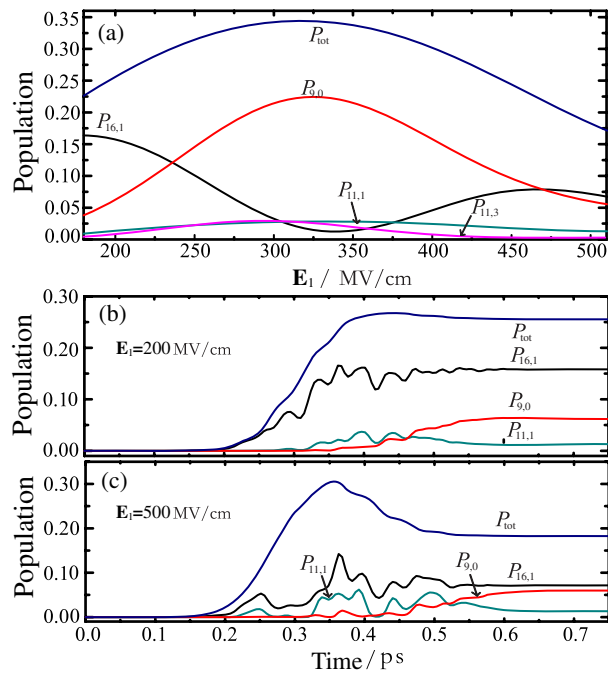


Fig. 3. Time-dependent population distributions versus the amplitude  $E_1$  of the first pulse for the target state  $|9,0\rangle$ .

probability between the states  $|16,1\rangle$  and  $|11,1\rangle$ . Therefore, the final population of the target state  $|9,0\rangle$  is only 0.062 and about 15.8% of the population stays in the state  $|16,1\rangle$ . For  $E_1 = 500$  MV/cm,  $P_{tot}$  reaches the maximal value at  $t = 0.36$  ps and then decreases to 0.183, as shown in Fig. 3(c). This indicates that part of the product molecules are dissociated again as the pulse amplitude is increased, which leads to the decrease in the total yield.

Figure 4(a) shows the relation between the rovibrational population and the second pulse amplitude  $E_2$ . It can be seen that the variation of  $P_{tot}$  is not obvious, which indicates that the amplitude  $E_2$  has a weak effect on the total yield. When  $E_2$  increases from 10 MV/cm to 140 MV/cm, the target population  $P_{9,0}$  increases with the decrease of the population  $P_{11,1}$ . When  $E_2 > 140$  MV/cm,  $P_{9,0}$  decreases from the maximal value to 0.064 and  $P_{11,1}$  increases from nearly zero to 0.063. The populations  $P_{16,1}$  and  $P_{11,3}$  increase slowly with the variation of  $E_2$ . The time-dependent population distributions for  $E_2 = 10$  MV/cm and 250 MV/cm are shown in Figs. 4(b) and 4(c), respectively. When  $E_2 = 10$  MV/cm, the intensity of the second pulse is weak and only a small amount of population can be transferred from the state  $|11,1\rangle$  to the state  $|9,0\rangle$ . As the two pulses are turned off, a large amount of population stays in the state  $|11,1\rangle$  and the population in the target state  $|9,0\rangle$  is nearly zero. When  $E_2 = 250$  MV/cm, the intensity of the second pulse is strong and part of population in the state  $|9,0\rangle$  is excited to high rovibrational levels, which leads to the increase of the populations in the states  $|11,1\rangle$  and  $|16,1\rangle$ . The oscillation amplitudes of the population curves in Fig. 4(c) are larger than those in Fig. 4(b). This indicates that the population transfer among the rovibrational levels is increased

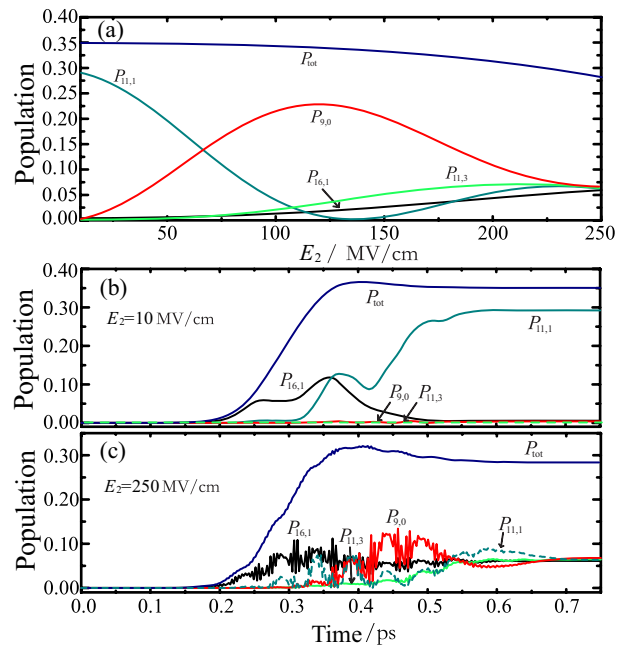


Fig. 4. Time-dependent population distributions versus the amplitude  $E_2$  of the second pulse for the target state  $|9,0\rangle$ .

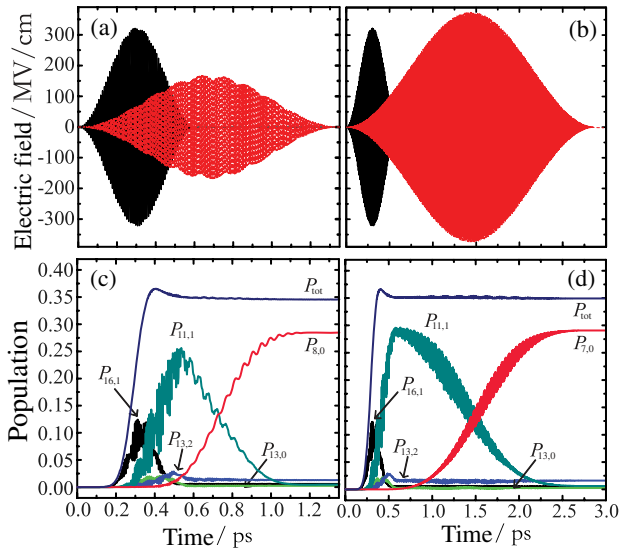


Fig. 5. Processes of PA for the target states  $|8,0\rangle$  and  $|7,0\rangle$  in two laser pulses. (a) The total electric field for the target state  $|8,0\rangle$ . The parameters of the second pulse are  $E_2 = 168.69$  MV/cm,  $\tau_2 = 1.35$  ps,  $t_2 = 0$  ps, and  $\omega_2 = 6528.29$   $\text{cm}^{-1}$ . (b) The total electric field for the target state  $|7,0\rangle$ . Parameters of the second pulse are  $E_2 = 374.38$  MV/cm,  $\tau_2 = 2.88$  ps,  $t_2 = 0$  ps, and  $\omega_2 = 9056.01$   $\text{cm}^{-1}$ . (c) and (d) The time-dependent population distributions for rovibrational states.

as the intensity of the second pulse increases. Therefore, about 6% of the population is transferred to the background state  $|11,3\rangle$  in Fig. 4(c).

Figure 5 is the PA reactions for the target states  $|8,0\rangle$  and  $|7,0\rangle$  in which the parameters of the first pulse are the same as in Fig. 2. The state-selectivities for the states  $|8,0\rangle$  and  $|7,0\rangle$  are  $P_{8,0}/P_{\text{tot}} = 82\%$  and  $P_{7,0}/P_{\text{tot}} = 83\%$ , respectively. The total yields  $P_{\text{tot}}$  in Fig. 5 are nearly the same as that in Fig. 2, but the state-selectivities are increased. As the vibrational quantum number of the target state is decreased, the energy gaps of adjacent levels are increased, which can reduce the transition probability of the background states and increase the state-selectivity. Compared with Fig. 2, the amplitudes and durations of the second pulses in Figs. 5(a) and 5(b) are increased. For a transition between two bound levels in a single electric state, the transition probability is decreased with increasing the difference of vibrational quantum numbers between these two bound levels<sup>[33]</sup>. As the transition  $|11,1\rangle \rightarrow |9,0\rangle$  is replaced by the transition  $|11,1\rangle \rightarrow |8,0\rangle$  or  $|11,1\rangle \rightarrow |7,0\rangle$ , the amplitude and duration of the second pulse have to be increased to maintain a high transition probability. Because the durations of the second pulses are increased, the overlapping regions of the two pulses in Figs. 5(a) and 5(b) are smaller than that in Fig. 2(a) and the maximum populations for the intermediate state  $|11,1\rangle$  in Figs. 5(c) and 5(d) are larger than that in Fig. 2(b).

It can be seen from the above cases that the amplitude of the second pulse increases rapidly with the decrease of the vibrational quantum number of the target state.

To produce the molecules in a lower state, we employ four pulses and the PA reaction is achieved through three intermediate states. The reverse ladder transition is

$$\begin{aligned} \text{continuum state} &\xrightarrow{\omega_1} |16,1\rangle \xrightarrow{\omega_1} \left\{ \begin{array}{l} |13,0\rangle \\ |13,2\rangle \end{array} \right\} \\ &\xrightarrow{\omega_1} |11,1\rangle \xrightarrow{\omega_2} \left\{ \begin{array}{l} |9,0\rangle \\ |9,2\rangle \end{array} \right\} \xrightarrow{\omega_2} |7,1\rangle \xrightarrow{\omega_3} \left\{ \begin{array}{l} |5,0\rangle \\ |5,2\rangle \end{array} \right\} \\ &\xrightarrow{\omega_3} |3,1\rangle \xrightarrow{\omega_4} \left\{ \begin{array}{l} |2,0\rangle \\ |2,2\rangle \end{array} \right\} \xrightarrow{\omega_4} |1,1\rangle \xrightarrow{\omega_4} |0,0\rangle. \end{aligned} \quad (6)$$

The parameters of the first pulse are the same as in Fig. 2 and the parameters of the other three pulses are chosen as:  $E_2 = 204.69$  MV/cm,  $\tau_2 = 1.48$  ps,  $t_2 = 0$  ps,  $\omega_2 = 4513.96$   $\text{cm}^{-1}$ ;  $E_3 = 333.24$  MV/cm,  $\tau_3 = 2.83$  ps,  $t_3 = 0$  ps,  $\omega_3 = 5949.06$   $\text{cm}^{-1}$ ;  $E_4 = 139.89$  MV/cm,  $\tau_4 = 2.64$  ps,  $t_4 = 0.97$  ps, and  $\omega_4 = 3613.98$   $\text{cm}^{-1}$ . The total electric field of four laser pulses is shown in Fig. 6(a).

Figure 6(b) shows the process of PA reaction in four pulses. It can be seen that the populations of the three intermediate states increase first and then decrease in the proper order, which describes the process of the reverse ladder transition. The total yield in Fig. 6(b) decreases slowly, which indicates that the PA process is accompanied by the PD reaction. If the population is transferred to a lower vibrational level, the PD probability of the product molecules will be decreased<sup>[34]</sup>. So, the lower the vibrational level of the population is, the slower the decreasing speed of the curve  $P_{\text{tot}}$  becomes, as shown in Fig. 6(b). When the four pulses are turned off, the state-selectivity is 87%. It can be seen from the four target states  $|9,0\rangle$ ,  $|8,0\rangle$ ,  $|7,0\rangle$ , and  $|0,0\rangle$  that the state-selectivity is increased with the decrease of the vibrational quantum number of the target state.

In conclusion, the two and four laser pulses are respectively used to produce the OH molecules in four different

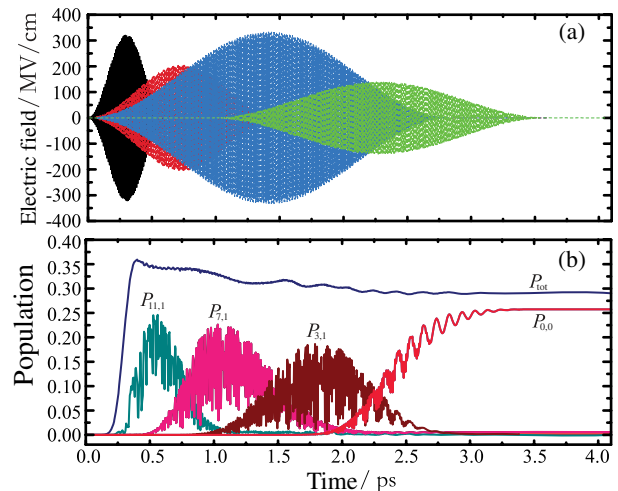


Fig. 6. Process of PA for the target state  $|0,0\rangle$  in four laser pulses. (a) The total electric field of four laser pulses. (b) The time-dependent population distributions for rovibrational states.

target states through the reverse ladder transition. The calculated results show that two or more pulses can induce the population transferring from a high rovibrational state to a low rovibrational state via one or more intermediate states. For the PA reaction in two pulses, the population of the target state depends on the amplitudes of the two pulse. The first pulse amplitude has an obvious effect on the total yield, but the effect of the second pulse amplitude on the total yield is weak. As a high level is chosen as the target state, the transition probability of the background states is large and the state-selectivity of the target state is low. The total yield induced by four pulses is smaller than that induced by two pulses, but the product molecules in a low rovibrational level can be obtained in four pulses and the state-selectivity of the target state is high.

This work was supported by the National Natural Science Foundation of China (No. 11347012) and the Natural Science Foundation of Liaoning Province of China (No. 20170540135).

## References

1. K. Bergmann, H. Theuer, and B. W. Shore, *Rev. Mod. Phys.* **70**, 1003 (1998).
2. C. Brif, R. Chakrabarti, and H. Rabitz, *New J. Phys.* **12**, 075008 (2010).
3. X. Ma, C. Yang, M. Wang, Y. Gong, and W. Liu, *Chin. Opt. Lett.* **10**, 110201 (2012).
4. K. Aikawa, D. Akamatsu, M. Hayashi, K. Oasa, J. Kobayashi, P. Naidon, T. Kishimoto, M. Ueda, and S. Inouye, *Phys. Rev. Lett.* **105**, 203001 (2010).
5. W. Salzmann, U. Poschinger, R. Wester, M. Weidemüller, A. Merli, S. M. Weber, M. Sauer, M. Plewicky, F. Weise, A. M. Esparza, L. Wöste, and A. Lindinger, *Phys. Rev. A* **73**, 023414 (2006).
6. B. L. Brown, A. J. Dicks, and I. A. Walmsley, *Phys. Rev. Lett.* **96**, 173002 (2006).
7. X. Hu, T. Xie, Y. Huang, and S. Cong, *Phys. Rev. A* **89**, 052712 (2014).
8. M. V. Korolkov and B. Schmidt, *Chem. Phys. Lett.* **361**, 432 (2002).
9. J. Pérez-Ros, M. Lepers, and O. Dulieu, *Phys. Rev. Lett.* **115**, 073201 (2015).
10. S. Dutta, J. Lorenz, A. Altaf, D. S. Elliott, and Y. P. Chen, *Phys. Rev. A* **89**, 020702(R) (2014).
11. W. Gunton, M. Semczuk, N. S. Dattani, and K. W. Madison, *Phys. Rev. A* **88**, 062510 (2013).
12. J. Yuan, Z. Ji, Z. Li, Y. Zhao, L. Xiao, and S. Jia, *J. Chem. Phys.* **143**, 044311 (2015).
13. J. Deiglmayr, A. Grochola, M. Repp, K. Mörtlbauer, C. Glück, J. Lange, O. Dulieu, R. Wester, and M. Weidemüller, *Phys. Rev. Lett.* **101**, 133004 (2008).
14. P. Zabawa, A. Wakim, M. Haruza, and N. P. Bigelow, *Phys. Rev. A* **84**, 061401(R) (2011).
15. J. Banerjee, D. Rahmlow, R. Carollo, M. Bellos, E. E. Eyler, P. L. Gould, and W. C. Stwalley, *Phys. Rev. A* **86**, 053428 (2012).
16. Z. Ji, H. Zhang, J. Wu, J. Yuan, Y. Yang, Y. Zhao, J. Ma, L. Wang, L. Xiao, and S. Jia, *Phys. Rev. A* **85**, 013401 (2012).
17. D. B. Blasing, I. C. Stevenson, J. Pérez-Ros, D. S. Elliott, and Y. P. Chen, *Phys. Rev. A* **94**, 062504 (2016).
18. G. K. Paramonov and P. Saalfrank, *Phys. Rev. A* **79**, 013415 (2009).
19. P. Marguetand and V. Engel, *J. Phys. B* **41**, 074026 (2008).
20. E. A. Shapiro, M. Shapiro, A. Pe'er, and J. Ye, *Phys. Rev. A* **75**, 013405 (2007).
21. J. Li, Y. Huang, T. Xie, S. Chai, and S. Cong, *Commun. Comput. Phys.* **17**, 79 (2015).
22. E. F. de Lima, T. S. Ho, and H. Rabitz, *Chem. Phys. Lett.* **501**, 267 (2011).
23. Y. Niu, S. Wang, and S. Cong, *Chem. Phys. Lett.* **428**, 7 (2006).
24. M. V. Korolkov, J. Manz, G. K. Paramonov, and B. Schmidt, *Chem. Phys. Lett.* **260**, 604 (1996).
25. E. F. de Lima, T. S. Ho, and H. Rabitz, *Phys. Rev. A* **78**, 063417 (2008).
26. P. Marguetand and V. Engel, *J. Chem. Phys.* **127**, 084115 (2007).
27. M. V. Korolkov and G. K. Paramonov, *Phys. Rev. A* **57**, 4998 (1998).
28. Y. Niu, R. Wang, and M. H. Qiu, *Phys. Rev. A* **84**, 023406 (2011).
29. J. Wang, G. Yang, J. He, and J. Wang, *Chin. Opt. Lett.* **15**, 050203 (2017).
30. E. Luc-Koenig, M. Vatasescu, and F. Masnou-Seeuws, *Eur. Phys. J. D* **31**, 239 (2004).
31. K. Willner, O. Dulieu, and F. Masnou-Seeuws, *J. Chem. Phys.* **120**, 548 (2003).
32. X. Yuan, C. Liu, P. Wei, Z. Zeng, and R. Li, *Chin. Opt. Lett.* **14**, 030201 (2016).
33. M. V. Korolkov, Y. A. Logvin, and G. K. Paramonov, *J. Phys. Chem.* **100**, 8070 (1996).
34. F. E. de Lima and J. E. M. Hornos, *Chem. Phys. Lett.* **433**, 48 (2006).